Pergamon

J. Mech. Phys. Solids, Vol. 43, No. 2, pp. 261–274, 1995

0022–5096/95 $9.50 + 0.00

0022–5096(94)00058–1

DISCONTINUOUS CONSTITUTIVE RESPONSE OF BRITTLE MATRIX FIBROUS COMPOSITES

CRESCENTINO BOSCO and ALBERTO CARPINTERI

Politecnico di Torino, Department of Structural Engineering, 10129 Torino, Italy

(*Received* 27 *July* 1993; *in revised form* 25 *July* 1994)

ABSTRACT

A bridged-crack model is proposed in order to explain and reproduce the constitutive flexural response of brittle matrix fibrous composites. This response is often discontinuous owing to the presence of virtual catastrophic branches; i.e. snap-through with load-control and snap-back with deflection-control.

The bridging tractions are assumed as constant plastic forces, whereas the cracks run in an elastic brittle matrix. The bridged-crack model accounts very well for small-scale microstructural studies of fibre-reinforced materials, or in the case of a rather small number of reinforcements, rivets or patches. The bridged-crack model results approach those of the cohesive-crack model of the Dugdale type when the density of the bridging elements tends to infinity.

The role of size scale is fundamental for the global structural behaviour, which can range from ductile to catastrophic simply with the variation of a dimensionless brittleness number, which is a function of matrix toughness, reinforcement yielding or slippage limit, reinforcement volume fraction and characteristic structural size. When the matrix is over-reinforced, the case of brittle crack propagation across the specimen is predicted, while, at the same time, intact bridging ligaments remain over most of the crack wake.

1. INTRODUCTION

In the case of modern, high-technology composite materials, such as fibre-reinforced ceramics and metal-matrix composites, two alternative nonlinear crack models are used to analyse the failure process: (1) the bridged-crack model, and (2) the cohesive-crack model.

The *bridged-crack model* is defined as that for which the stress-intensity factor at the crack tip is not zero, $K_{I(tip)} = K_{IC}$ being the criterion for crack growth. Different versions of the model have been used to describe microcracking of fibre-reinforced materials (Cox, 1991; Cox and Lo, 1992; Marshall *et al.*, 1985; Budiansky *et al.*, 1986; Foote *et al.*, 1986; Jenq and Shah, 1985; Kendall *et al.*, 1991), as well as macrocracking of materials reinforced by a rather small number of elements as rivets or patches (Carpinteri, 1984; Carpinteri and Carpinteri, 1984; Bosco and Carpinteri, 1992a,b).

The *cohesive-crack model*, on the other hand, is defined as that for which the stress field is nonsingular everywhere along the fracture zone, $K_{I(tip)} = 0$, the criterion for crack growth being in this case a stress-criterion (Dugdale, 1960; Barenblatt, 1962; Willis, 1967; Rice, 1968; Bilby *et al.*, 1963; Smith, 1989; Carpinteri, 1989a,b). In a cohesive-crack model, the damage process producing the advance of the cohesive

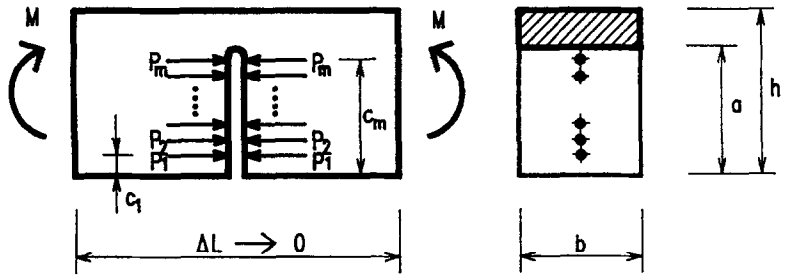

Fig. 1. Cracked element and position of reinforcements.

zone is the same as that governing the opening process along the whole cohesive zone. This is true, for instance, for materials with a high density of fibres, whereas it is not true, for example, for steel bar reinforced concrete (Bosco *et al.*, 1990a,b). In any case it is only a matter of scale of observation. For relatively small scales, the crack growth is governed by the toughness of the matrix, while the stress vs displacement cohesive relation is governed by the properties of the reinforcing phase and how it is coupled to the matrix.

In the present paper, a bridged-crack model is proposed which is able to explain and reproduce the constitutive flexural response of brittle matrix fibrous composites (Carpinteri, 1984; Carpinteri and Carpinteri, 1984; Bosco and Carpinteri, 1991, 1992a,b). This response is often discontinuous owing to the presence of virtual catastrophic branches; i.e. snap-through branches with load-control, and snap-back branches with deflection-control (Bosco and Carpinteri, 1991, 1992a,b).

The bridging tractions are assumed as constant plastic forces, whereas the crack runs in an elastic brittle matrix. The effect of the size scale is found to be fundamental for the global structural behaviour, which can range from ductile to catastrophic simply with the variation of a dimensionless brittleness number, which is a function of the toughness of the matrix, of the yielding or slippage limit of the reinforcement, of the volume fraction of the reinforcement, and of a characteristic structural size (Carpinteri, 1982, 1989a,b). When the matrix is over-reinforced, the crack propagates in a brittle manner across the specimen, while the bridging elements remain intact over most of the crack wake.

2. THEORETICAL MODEL

Consider the problem of a cracked element loaded by n independent generalized actions $Q_1, Q_2, \ldots, Q_n$ (Fig. 1).

Let $w_1, w_2, \ldots, w_n$ be the generalized displacements of their points of application. The generic displacement, via application of the superposition principle, can be expressed as

$$w_i = \sum_{j=1}^{j=n} \lambda_{ij} Q_j \quad (i = 1, 2, \ldots, n), \tag{1}$$

where λ_{ij} represents the compliance (influence coefficient) measured at point i, due to the action Q_j applied at point j. According to Betti's Theorem $\lambda_{ij} = \lambda_{ji}$.

In the case of Mode I crack propagation, the strain energy release rate is given by (Okamura *et al.*, 1973, 1975)

$$G = \frac{1}{2}\sum_{i=1}^{i=n}\sum_{j=1}^{j=n} Q_i Q_j \frac{\mathrm{d}\lambda_{ij}}{\mathrm{d}A} = \frac{1-\nu^2}{E} K_{\mathrm{I}}^2, \tag{2}$$

where

$$K_{\mathrm{I}} = \sum_{k=1}^{k=n} K_{\mathrm{I}k} \tag{3}$$

is equal to the sum of all the stress-intensity factors $K_{\mathrm{I}k}$ due to all the actions Q_k.

If the element is subjected to a bending moment M and to m concentrated loads $P_1, P_2, \ldots, P_m$ applied on the surfaces of the crack at distances $c_1, c_2, \ldots, c_m$ from the lower edge of the beam (Fig. 1), the variation ΔW.of the total potential energy is given by

$$\Delta W = \int_0^{c_1} G_M b\,\mathrm{d}a + \int_{c_1}^{c_2} G_{(M+P_1)} b\,\mathrm{d}a + \int_{c_2}^{c_3} G_{(M+P_1+P_2)} b\,\mathrm{d}a + \cdots + \int_{c_m}^{a} G_{(M+P_1+P_2+\cdots+P_m)} b\,\mathrm{d}a. \tag{4}$$

The application of the superposition principle leads to the following expression (Bosco and Carpinteri, 1992a):

$$\frac{K_i K_j}{E} = \frac{1}{2} P_i P_j \frac{\mathrm{d}\lambda_{ij}}{\mathrm{d}A}, \tag{5}$$

where $\mathrm{d}A = b\,\mathrm{d}a$, and the compliance λ_{ij} is given by

$$\lambda_{ij} = \int_{c_j}^{a} \mathrm{d}\lambda_{ij} = \frac{2}{E}\int_{c_j}^{a} \frac{K_i K_j}{P_i P_j}\mathrm{d}A \quad (i<j). \tag{6}$$

Taking into account that

$$K_{\mathrm{I}M} = \frac{M}{bh^{3/2}} Y_M(\xi) \tag{7}$$

and that

$$K_{\mathrm{I}P_i} - \frac{P_i}{bh^{1/2}} Y_P\left(\frac{c_i}{h}, \xi\right), \quad (i = 1, 2, \ldots, m), \tag{8}$$

the compliances related to the loads, and referred to a generic relative crack length $a/h = \xi$, are expressed as

$$\lambda_{ij} = \frac{2}{bE}\int_{c_j/h}^{\xi} Y_P\left(\frac{c_i}{h}, \xi\right) Y_P\left(\frac{c_j}{h}, \xi\right) \mathrm{d}\xi, \quad (i < j, \quad c_i < c_j) \tag{9}$$

with $\lambda_{ij} = \lambda_{ji}$, while the compliances related to the moment are

$$\lambda_{i0} = \frac{2}{bhE}\int_{c_j/h}^{\xi} Y_P\left(\frac{c_i}{h}, \xi\right) Y_M(\xi)\, \mathrm{d}\xi, \quad (i = 1, 2, \ldots, m), \tag{10}$$

$$\lambda_{00} = \frac{2}{bh^2E}\int_0^{\xi} Y_M^2(\xi)\, \mathrm{d}\xi, \tag{11}$$

Y_P and Y_M being the shape functions of the relative crack depth $\xi = a/h$, and of the distance c_i of the fibre $i\,(i = 1, 2, .., m)$ from the lower edge of the beam, respectively (Carpinteri, 1981, 1984).

Observe that point forces on the crack faces give rise to a logarithmic displacement, so that a further simplifying assumption is involved. If a condition of zero displacement between the crack faces is imposed, this would need to be applied over a finite length, and not merely at a point. Thus, the assumed width of the fibres will be equal to 10^{-5} of the beam depth.

3. DISPLACEMENT COMPATIBILITY CONDITIONS

Let the stress–strain constitutive law of fibres be rigid–perfectly plastic, while the matrix behaves linearly. Consequently, the relationships between M, $P_1, P_2, \ldots, P_m$ are represented by compatibility conditions that correspond to relative displacements w of the points of application of the loads on the crack surfaces. Displacements greater than zero are thus only allowed when the yielding limit of the fibres is reached, or when the slippage due to local debonding between the fibres and the matrix occurs. Then it follows, for the generic equation $(1 \leqslant j \leqslant m)$ that

$$w_j = \lambda_{j0} M - \lambda_{j1} P_1 - \lambda_{j2} P_2 - \cdots - \lambda_{jm} P_m = 0 \tag{12}$$

and, in matrix form

$$\{w\} = \{\lambda_0\}\, M - [\lambda]\, \{P\} = \{0\}, \tag{13}$$

where $[\lambda]$ is the matrix of influence coefficients related to the reactions $P_1, P_2, \ldots P_m$ (vector $\{P\}$) of the fibres (tending to close the crack), while the corresponding influence coefficients related to bending moment are grouped in the vector $\{\lambda_0\}$.

The relationships (13) allow us to consider a general problem because we have not laid any restriction on the actual cross-sectional area of each fibre.

Up to the yielding limit, f_y, in the outermost fibre of area A_{s1} $(P_1 = P_{P1} = A_{s1} f_y)$, and when the applied moment does not produce crack propagation, the dimensionless reactions of the fibres are obtained from (12). When the yielding limit has been reached, the remaining equations (12) (from the second to the last) contain P_{P1} instead of P_1. Thus for $M_{P1} < M < M_{P2}$, the generic equation in which $1 < j \leqslant m$ becomes

$$w_j = \lambda_{j0}M - \lambda_{j1}P_{P1} - \lambda_{j2}P_2 - \lambda_{j3}P_3 - \cdots - \lambda_{jm}P_m = 0, \tag{14}$$

while the first equation gives $w_1 > 0$.

When also the second fibre has yielded, we have $P_2 = P_{P2} = A_{s2}f_y$, and for $M_{P2} < M < M_{P3}$, we have (for $2 < j \leqslant m$)

$$w_j = \lambda_{j0}M - \lambda_{j1}P_{P1} - \lambda_{j2}P_{P2} - \lambda_{j3}P_3 - \cdots - \lambda_{jm}P_m = 0, \tag{15}$$

whilst both w_1 and w_2 are greater than zero, and so forth until the last fibre has yielded.

In actual fact, for a given crack length ξ, with the position

$$\frac{P_i h}{M} = \frac{1}{r_i} \quad (i = 1, 2, \ldots, m), \tag{16}$$

the system (12) provides the dimensionless reactions of the fibres, in the form

$$\frac{h}{M}\{P\} = \left\{\frac{1}{r}\right\} = [\lambda]^{-1}\{\lambda_0\}h. \tag{17}$$

In the same way we can obtain the bending moment of plastic flow for each fibre. This is possible by substituting $M = M_{Pi}$ in the systems represented by the equations (14), (15), etc.

Taking into account the position

$$N_{P_i} = \frac{f_y h^{0.5}}{K_{IC}} \frac{A_{si}}{A} = \frac{h^{0.5}}{K_{IC}A} P_{P_i}, \tag{18}$$

we must consider that when the generic fibre j yields, we have $M = M_{P_j}$, while, at the same time, the force transmitted by the fibre $i\,(i < j)$ is P_{P_i}. If we consider (18), this force can be expressed as

$$\frac{P_{P_i}}{P_{P_j}} = \frac{N_{P_i}}{N_{P_j}} \tag{19}$$

and (16) gives $P_{P_i} = \dfrac{M_{P_i}}{h}\dfrac{1}{r_j}\dfrac{N_{P_i}}{N_{P_j}}$.

In this way we can rewrite the generic equation of the system (12) or (13), where, for the generic bending moment of plastic flow M_{P_j}, the dimensionless reactions $1/r_j$ are obtained

$$\lambda_{j0}h - \lambda_{j1}\frac{1}{r_j}\frac{N_{P1}}{N_{Pj}} - \lambda_{j2}\frac{1}{r_j}\frac{N_{P2}}{N_{Pj}} - \cdots - \lambda_{j(m-1)}\frac{1}{r_{m-1}} - \lambda_{jm}\frac{1}{r_m} = 0. \tag{20}$$

4. CRACK PROPAGATION

If M_F denotes the value of M for quasi-static crack growth, i.e. such that $K_I = K_{IC}$, from (7) and (8) it follows that

$$M_F = \frac{K_{IC} b h^{3/2}}{Y_M(\xi)} + \sum_{i=1}^{i=m} \frac{Y_{P_i}\left(\frac{c_i}{h}, \xi\right)}{Y_M(\xi)} P_i h. \tag{21}$$

Taking into account that in the elastic range and up to $M \leqslant M_{Pi}$ we have $P_i/P_{Pi} = M/M_{Pi}$ with $P_i = \alpha_i P_{Pi}$ and $\alpha_i = P_i/P_{Pi} < 1$, (21) in nondimensional form becomes

$$\frac{M_F}{K_{IC} b h^{3/2}} = \frac{1}{Y_M(\xi)} + \frac{N_P}{Y_M(\xi)\rho} \sum_{i=1}^{i=m} Y_{P_i}\left(\frac{c_i}{h}, \xi\right) \alpha_i \rho_i, \tag{22}$$

where $N_P = f_y \rho h^{1/2}/K_{IC}$ is the brittleness number (Carpinteri, 1981, 1984), in which the yielding limit of the fibre f_y, the critical value of the stress-intensity factor K_{IC}, and the total percentage of fibre in the cross section $\rho = \Sigma \rho_i = (\Sigma A_{si})/bh$ are involved. In (22), $\rho_i = A_{si}/bh$ represents the percentage of each fibre, and in any case, referred to the whole area bh of the cross-sectional matrix, while $\alpha_i (i = 1, 2, \ldots, m)$ assumes the value 1 if $M_F > M_{Pi}$, or M_F/M_{Pi} if $M_F \leqslant M_{Pi}$.

5. STRUCTURAL RESPONSE OF THE CRACKED ELEMENT

The knowledge of the ratio M_F/M_{Pi}, between the moment of crack propagation M_F (for the generic relative crack depth ξ) and the bending moment of plastic flow M_{Pi} (of the generic fibre i), allows determination of the structural response of the cracked element in terms of local rotation. In fact the force transmitted by the fibre i is $P_i = P_{Pi}(M_F/M_{Pi})$, while the local rotation due to the presence of the crack may be obtained by superposition, as follows:

$$\Delta\varphi_F = \lambda_{00} M_F - \sum_{i=1}^{i=m} \lambda_{i0} P_{P_i} \alpha_i, \tag{23}$$

where λ_{i0} and λ_{00} are expressed by (10) and (11), and α_i has the meaning already mentioned above.

Let $\Delta\varphi_F$ be the rotation obtained from (23) for a given relative crack depth ξ when the corresponding moment of crack propagation $M = M_F$ is reached, and let $\Delta\varphi_{F0}$ be the rotation obtained for the initial relative crack depth ξ_0 when the first moment of crack propagation is reached. It is then possible to obtain the normalized moment–rotation diagram in relation to the crack depth increase, in the range between ξ_0 and 0.7, the latter being the maximum value for which $Y_M(\xi)$ is defined.

In what follows, the applicability of the model is shown for the cases of two and a very large number of fibres.

6. TWO FIBRES

Let the cracked beam element be subjected to the bending moment M, while the fibres transmit to the adjacent matrix surfaces a statically indeterminate axial force equal to

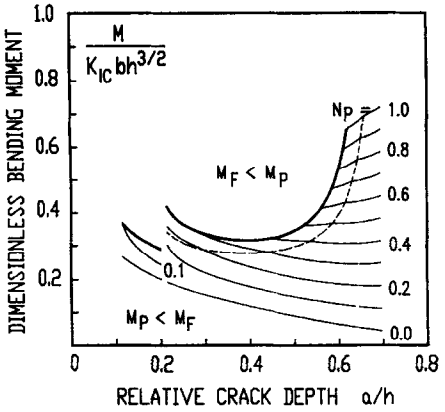

Fig. 2. Bending moment of crack propagation versus relative crack depth (two layers of reinforcement).

$$P_i = \sigma_{si} A_{si} \quad (i = 1, 2), \tag{24}$$

A_{si} being the cross-sectional area of the fibre i and σ_{si} the related stress.

If the displacement discontinuity in the cracked cross-section at the level of the outermost fibre is assumed to be zero up to the moment of yielding or slippage of the fibre ($P_1 = P_{P1} = A_{s1} f_y$), and when the applied moment does not produce crack propagation (Bosco, 1990), the displacement compatibility conditions

$$\begin{aligned} w_1 &= \lambda_{10} M - \lambda_{11} P_1 - \lambda_{12} P_2 = 0, \\ w_2 &= \lambda_{20} M - \lambda_{21} P_1 - \lambda_{22} P_2 = 0, \end{aligned} \tag{25}$$

allow us to obtain the unknown forces P_1 and P_2 as functions of the applied moment M. When the yielding limit has been reached, the second of equations (25) contains P_{P1} instead of P_1, while w_1 (greater than zero) is given by the first of the same equations (25) by substituting $P_1 = P_{P1}$. Then, when both fibres have yielded ($P_1 = P_{P1}$ and $P_2 = P_{P2}$), both w_1 and w_2 are greater than zero.

At crack propagation, when the critical value of the stress-intensity factor is reached ($K_I = K_{IC}$ and $M = M_F$), (22) gives

$$\frac{M_F}{K_{IC} b h^{3/2}} = \frac{1}{Y_M(\xi)} + \frac{N_P}{Y_M(\xi)\rho}\left[Y_P\left(\frac{c_1}{h}, \xi\right)\alpha_1 \rho_1 + Y_P\left(\frac{c_2}{h}, \xi\right)\alpha_2 \rho_2 \right], \tag{26}$$

where $\rho_i = A_{si}/bh$ represents the percentage of each of the two fibres, in every case referred to the whole area bh of the cross section, and α_i ($i = 1, 2$) assumes the value 1 if $M_F > M_{Pi}$, and M_F/M_{Pi} if $M_F \leqslant M_{Pi}$.

In this case, functions (26) are represented in Fig. 2 against the variation of the initial relative crack depth ξ ($\xi > c_1/h = 0.1$, while $c_2/h = 0.2$), and with the brittleness number N_P varying, in the case $A_{s1} = A_{s2} = A_s$ and thus $\rho = 2A_s/bh$.

First of all, it is evident that for values of N_P greater than $\cong 0.20$, the second fibre increases the strength of the cross section, since relative crack propagation from $\xi = 0.2 - \varepsilon$ to $\xi = 0.2 + \varepsilon$ is possible only by increasing the applied bending moment to a value greater than that causing crack initiation.

As regards the fibre conditions, from the lower part of the diagram it emerges that crack propagation occurs when both fibres have yielded only for very low values of N_P, as shall appear more clearly subsequently, i.e. for small percentages of fibre or deep cross sections. On the other hand, if the initial crack depth is sufficiently limited ($\xi < 0.25$), crack propagation can occur with the fibre in the elastic condition for values of N_P greater than $\cong 0.30$. Moreover it should be pointed out that, for small values of N_P ($N_P < 0.3$), the phenomenon of crack propagation is in every case unstable, the slope of the curves $N_P = \text{const.}$ being negative right up to the value $\xi = 0.7$.

On the other hand, if the various values of crack depth are interpreted as an evolving phenomenon of cracking, i.e. when the parameter ξ gives the successive positions of the crack tip, the necessity emerges of reducing the bending moment to avoid a very fast propagation followed by a sudden failure of the element.

For values of N_P greater than $\cong 0.3$ (see again Fig. 2), the crack propagation develops in an unstable manner until the relative crack depth corresponds to the value for which the curve $N_P = \text{const.}$ presents a minimum. Beyond that point it is again necessary to supply energy to induce further increase of cracking. As a final consideration regarding a directly applied load, we can define the global crack propagation as stable if, for $\xi = 0.7$, the diagram does not present a value lower than that corresponding to the initial propagation. The model thus predicts that the crack propagation phenomenon is stable only for sufficiently high values of initial crack depth ($\xi = 0.5 \div 0.6$), or that it may become stable only for values of N_P greater than $\cong 0.3$.

The local rotation $\Delta\varphi_F$, due to the presence of a crack, for a given relative crack depth ξ, when $M = M_F$, is obtained as indicated in (23)

$$\Delta\varphi_F = \lambda_{00}M_F - \lambda_{10}P_1 - \lambda_{20}P_2 = \lambda_{00}M_F - \lambda_{10}P_{P1}\alpha_1 - \lambda_{20}P_{P2}\alpha_2. \tag{27}$$

If $\Delta\varphi_{F0}$ is the rotation obtained for the initial relative crack depth ξ_0, when $M = M_F$, we obtain the normalized moment–rotation diagram for the range $\xi = \xi_0$ to $\xi = 0.7$, the latter being the maximum value for which $Y_M(\xi)$ is defined. In the present case $\xi_0 = c_1/h = 0.1$ has been assumed.

In Figs 3(a)–3(f) the moment–rotation diagrams are shown for $N_P = 0$ (no fibre), 0.1, 0.2, 0.4, 0.7 and 1.0, respectively. The same diagrams also show the ultimate carrying capacity when the cross section is completely cracked (dotted horizontal asymptotes) and both fibres have yielded. In this connection, since the maximum resultant tensile force of the two fibres (having the same area A_s) is located at $d = [1-(c_1+c_2)/2h]h = \delta h$ from the upper edge of the cross section, the ultimate bending moment turns out to be $M_u = 2P_P h\delta$. Considering that $P_{P1} = P_{P2} = P_P$ and therefore $N_P = 2P_P h/(K_{IC}bh^{3/2})$, it is possible to obtain $M_u/(K_{IC}bh^{3/2}) = N_P\delta$, which is the limit value to which the normalized moment–rotation curves tend, for every given value of N_P. It is worth noting that for sufficiently high matrix strength and sufficiently low percentage of fibre this type of failure precedes crushing of the matrix.

From Figs 3(a)–3(f), the following may be observed.

(a) For $N_P = 0$, i.e. no fibre, while the bending moment M increases from zero to M_F and the relative crack depth ξ remains constant ($\xi_0 = 0.1$), the normalized rotation

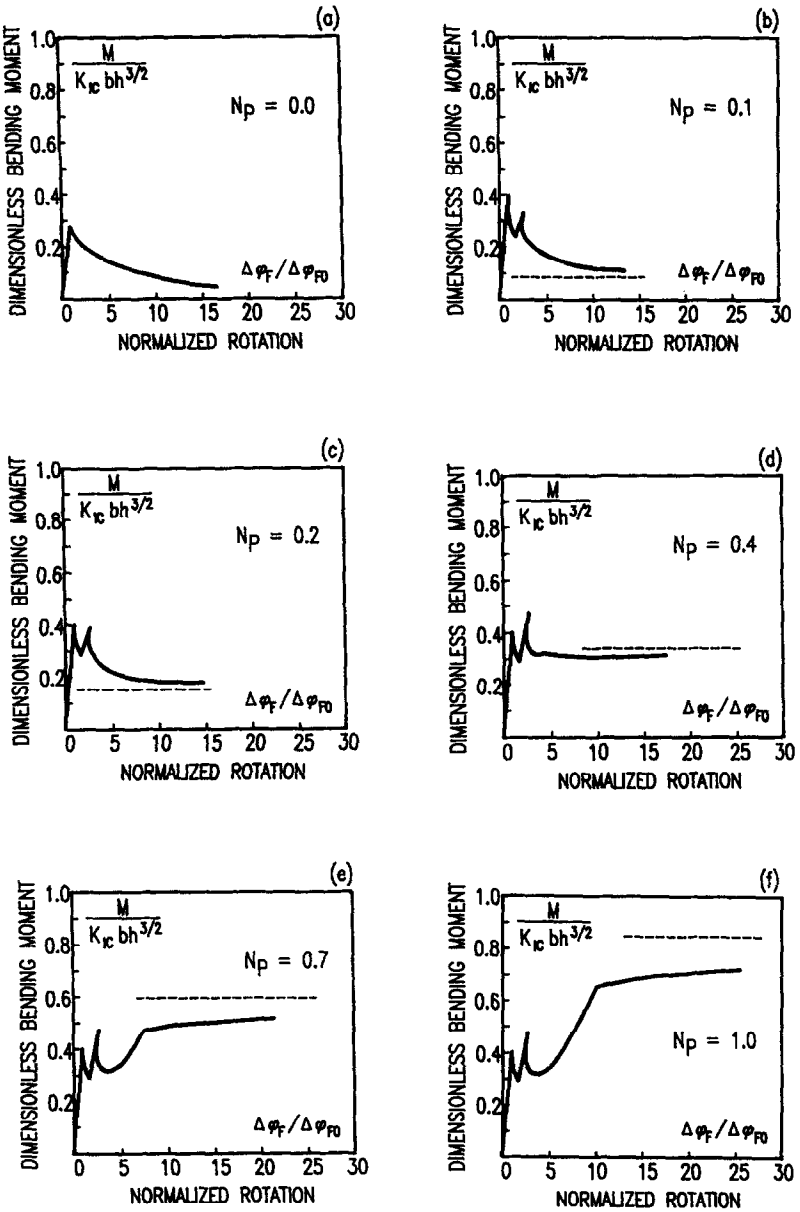

Fig. 3. Normalized moment–rotation diagrams (two layers of reinforcement).

$\Delta\varphi_F/\Delta\varphi_{F0}$ varies from 0 to 1. Once crack propagation has occurred, there is no possibility of increasing the resistance, and both Figs 3(a) and 3(b) decrease (bold curve) down to complete failure of the element.

(b) In Fig. 3(b) where the case $N_P = 0.1$ is presented, this value of N_P represents either very low percentage of fibre or deep cross section.

When crack propagation starts, we note that once again it is not possible to increase

the resistance, and the relative crack depth a/h grows, following the curve $N_P = 0.1$, up to the value $\xi = 0.7$.

The contribution of the second fibre does not involve any increase of load-bearing capacity with regard to the moment of initial crack propagation. Hence the global phenomenon is unstable.

A final remark concerns the fibre conditions during crack propagation from $\xi = 0.1$ to $\xi = 0.7$, that occur simultaneously with the yielding of the fibre, both when $\xi = 0.1$ (first fibre) and when $\xi = 0.2$ (second fibre).

(c) In Fig. 3(c) (where $N_P = 0.2$ is considered) no substantial modifications in the global behaviour emerge with respect to the case of $N_P = 0.1$. In fact the phenomenon is still globally unstable, even though the second peak of bending moment is approximately at the same level as the first and crack propagation develops when the first fibre is still elastic [the transitional curve in the left-hand part of the diagram of Fig. 3(b) is reached before the non-plotted curve corresponding to $N_P = 0.2$]. However, it should be pointed out that the first fibre yields simultaneously with the cross-propagation through the second fibre (peak of bending moment at $\xi = 0.2$) and that the second one yields at the cuspidal point on the curve $N_P = 0.2$.

(d) In Fig. 3(d) (where $N_P = 0.4$ is considered) the benefit of the second fibre emerges, the second moment of crack propagation being greater than the first. Nevertheless, the ultimate resistant bending moment does not reach any of the peaks, and so the phenomenon is still globally unstable.

(e) In Fig. 3(e) ($N_P = 0.7$) on the other hand, the bending moment at $\xi = 0.7$, is greater than M_F (whichever of the two peaks of crack propagation is considered). This means that the global process of crack propagation is no longer brittle and can only be obtained by increasing the applied external moment after the second peak has been reached.

(f) For $N_P = 1.0$ [Fig. 3(f)] the same considerations that apply for $N_P = 0.7$ can be developed; hence for sufficiently high percentages of fibre the cracking of the cross section is globally stable.

In conclusion, it may thus be stated that when a given amount of fibre is distributed over a limited number of layers of equal area, the model represents the different failure mechanisms and their transition from unstable to stable crack propagation by means of the brittleness number N_P.

On the other hand, the apparent delay in reaching the stable condition at complete crack propagation (indicated by the dashed horizontal line of the ultimate bending moment M_u) is due not so much to the different distribution of the total amount of fibre as to the different position of the centroids with respect to the compression side (0.85 h in the present case).

7. LARGE NUMBER OF FIBRES

All the relationships from (12) to (23), both for displacement conditions and for crack propagation, hold good when the critical value of the stress-intensity factor is reached.

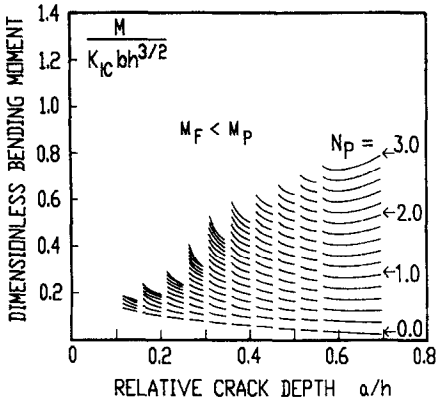

Fig. 4. Bending moment of crack propagation versus relative crack depth (10 layers of reinforcement).

In the case of a very large number of fibres (indicated with m), and for a distribution of the fibres between the relative crack depths $\xi_0 = c_1/h = 0.1$ and $c_m/h = 0.55$, functions (26) are represented in Fig. 4 against the variation of the initial relative crack depth ξ ($\xi > c_1/h = 0.10$), and with the brittleness number N_P varying, in the case $A_{s1} = A_{s2} = \cdots = A_{sm} = A_s$ and thus $\rho = mA_s/bh$ (Bosco and Carpinteri, 1991).

In Figs 5(a)–5(f) the moment–rotation diagrams are shown for $N_P = 0$, 0.2, 0.4, 0.8, 1.0 and 2.0 (the case $N_P = 0$ is not different from the previous one). The phenomenon of crack propagation in every case appears unstable between one fibre and another, whatever the position of two adjacent fibres, and can become stable only when $\xi > c_m/h$.

On the other hand, as discussed before, if the crack depth is interpreted as a parameter of the evolving phenomenon of crack growth, the necessity again appears of reducing the bending moment to avoid a very fast propagation followed by a sudden failure of the element. Furthermore, the model once again predicts that the crack propagation phenomenon can be globally stable only for sufficiently high values of crack depth ($\xi > 0.6$) and/or for values of N_P greater than $\cong 0.6$.

Analysis of the behaviour for various total percentages of fibre, except for $N_P = 0$, where, as is obvious, no changes occur with respect to the previous case, prompts the following remarks.

(a) All the diagrams given in Figs 5(a)–5(f) show an enveloping curve of the characteristic saw-toothed profile that indicates the evolution of crack propagation after the first peak. These profiles appear more regular and tend to become continuous as the fibres tend to become continuously distributed. All the diagrams are also characterized by the horizontal dashed line that represents the ultimate bending moment M_u at complete propagation of the crack (in the last diagram, for $N_P = 2.0$, the limit is not shown for reasons of convenience, and is equal to 1.35). Likewise for convenience, the points of yielding of the layers of fibre are no longer shown.

(b) As regards the global response of the cracked element, a comparison may readily be made between the ordinate at initial crack propagation and the horizontal dashed line mentioned above, which represents the ultimate resistance. In view of the

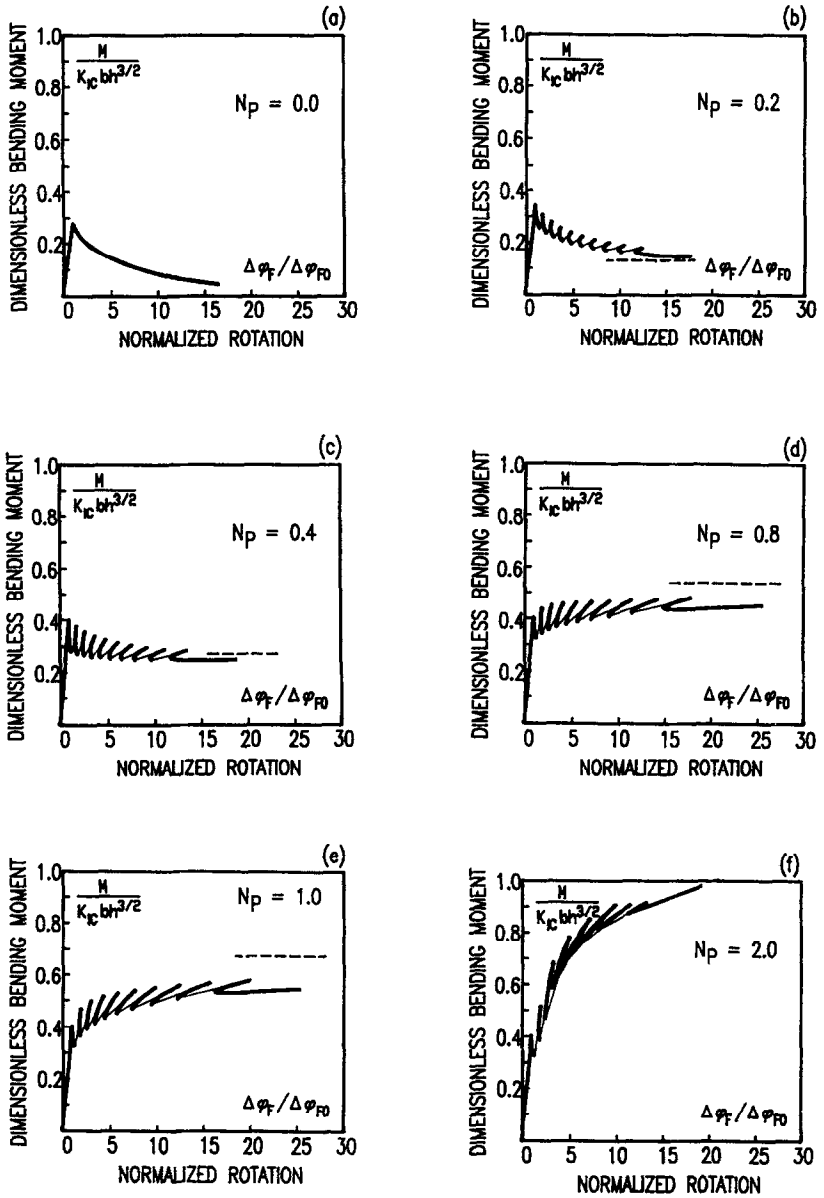

Fig. 5. Normalized moment–rotation diagrams (10 layers of reinforcement).

high number of fibres that may correspond to a continuous distribution of fibres, the local instabilities, revealed in every case by the discrete model, become meaningless, and only the locus of peaks needs be taken into account. Consequently we note that the global response shifts from brittle, as indicated in Fig. 5(c) (for $N_P < 0.5$), to stable (for $N_P > 0.6$), as represented in Figs 5(d)–5(f).

Once more it should be noted that it is not possible to make a direct comparison between the responses for different numbers of layers (for $N_P = \text{const.}$), because of the different position of the centroid of the fibre. However, also in the case of 10 fibres, when lower brittleness numbers N_P are involved, brittle crack propagation occurs, while for higher values of N_P, crack propagation is stable.

8. CONCLUSIONS

The approach adopted of using a bridged-crack model, where the forces transmitted by the fibres are directly applied to the crack surfaces, and of imposing appropriate displacement compatibility conditions, makes it possible to predict the different failure mechanisms of brittle-matrix fibrous composites as a function of both fibre content and size scale.

Bending moment versus rotation, with varying content and position of the fibres, is analysed for a given initial crack depth. Detailed examples are provided in the paper, along with extensive discussion of the various cases, also as regards the moment-rotation response, with particular attention drawn to the local and global instability of crack propagation. The subsequent yielding of the fibres is described in relation to the crack-evolution process and for various total fibre content.

The versatility of the model appears clearly both for discretely reinforced structures and for brittle matrix fibrous materials. In fact, for a limited number of fibres it is shown that the model can be usefully applied to the cases of steel bar reinforced concrete, for which its ability to represent the transition from brittle to ductile failure has been demonstrated (in particular the model represents consistently the experimental behaviour of specimens in which slippage or debonding of the reinforcements actually occurs). On the other hand, the case of a very large number of fibres is representative of continuous distributions and clearly illustrates the applicability of the model to fibre-reinforced materials.

In addition, the model provides information about the global crack propagation mode, which, in the cases analysed here, appears unstable for low values of N_P (low content of fibres or deep cross sections) or for limited relative crack depths. More precisely, crack propagation is stable only for relative crack depths greater than a minimum value (varying slightly with the number of fibres), or may become stable only for brittleness numbers greater than a definite value.

Snap-back and snap-through instabilities are predicted by varying the above-mentioned parameters, the former discontinuous response being highlighted by the deformation-controlled process and locally brittle behaviour, whereas the latter is brought out by the load-controlled process and globally ductile behaviour.

ACKNOWLEDGEMENTS

The authors gratefully acknowledge the financial support provided by the National Research Council (CNR) and the Department for the University and for Scientific and Technological Research (MURST) in order that this research be carried out.

REFERENCES

Barenblatt, G. I. (1962) *Advances in Applied Mechanics* (ed. H. L. Dryden and T. von Karman), pp. 55–129. Academic Press, New York.
Bilby, B. A., Cottrell, A. H. and Swinden, K. H. (1963) *Proc. R. Soc. London* **A272,** 304–314.
Bosco, C. (1990) *Eighth European Conf. Fracture*, pp. 811–817. Torino, Italy.
Bosco, C. and Carpinteri, A. (1991) *Int. Conf. Fracture Processes in Brittle Disordered Materials*, Vol. 1, pp. 295–305. Noordwijk, The Netherlands.
Bosco, C. and Carpinteri, A. (1992a) *Theor. Appl. Fract. Mech.* **17,** 61–68.
Bosco, C. and Carpinteri, A. (1992b) *J. Engng Mech.* **118,** 1564–1577.
Bosco, C., Carpinteri, A. and Debernardi, P. G. (1990a) *Engng Fract. Mech.* **35,** 665–677.
Bosco, C., Carpinteri, A. and Debernardi, P. G. (1990b) *J. Struct. Engng* **116,** 427–437.
Budiansky, B., Hutchinson, J. W. and Evans A. G. (1986) *J. Mech. Phys. Solids* **34,** 167–189.
Carpinteri, A. (1981) *IABSE Colloquium on Advanced Mechanics of Reinforced Concrete*, pp. 17–30. Delft, The Netherlands.
Carpinteri, A. (1982) *Engng Fract. Mech.* **16,** 467–481.
Carpinteri, A. (1984) *J. Struct. Engng* **110,** 544–558.
Carpinteri, A. (1989a) *J. Mech. Phys. Solids* **37,** 567–582.
Carpinteri, A. (1989b) *Int. J. Solids Struct.* **25,** 407–429.
Carpinteri, Al. and Carpinteri, An. (1984) *J. Struct. Engng* **110,** 2073–2084.
Cox, B. N. (1991) *Acta Metall. Mater.* **39,** 1198–1201.
Cox, B. N. and Lo, C. S. (1992) *Acta Metall. Mater.* **40,** 69–80.
Dugdale, D. S. (1960) *J. Mech. Phys. Solids* **8,** 100–104.
Foote, R. M. L., Mai, Y. W. and Cotterell, B. (1986) *J. Mech. Phys. Solids* **34,** 593–607.
Jenq, Y. S. and Shah, S. P. (1985) *J. Engng Mech.* **112,** 19–34.
Kendall, K., Clegg, W. J. and Gregory, R. D. (1991) *J. Mater. Sci. Lett.* **10,** 671–674.
Marshall, D. B., Cox, B. N. and Evans, A. G. (1985) *Acta Metall. Mater.* **33,** 2013–2021.
Okamura, H., Watanabe, K. and Takano, T. (1973) American Society for Testing and Materials, STP 536, pp. 423–438.
Okamura, H., Watanabe, K. and Takano, T. (1975) *Engng Fract. Mech.* **7,** 531–539.
Rice, J. R. (1968) *J. Appl. Mech.* **35,** 379–386.
Smith, E. (1989) *Int. J. Engng Sci.* **27,** 301–307.
Willis, J. R. (1967) *J. Mech. Phys. Solids* **8,** 151–162.